INTERNATIONAL JOURNAL OF AUTOMOTIVE AND MECHANICAL ENGINEERING
ISSN: 2229-8649 e-ISSN: 2180-1606
VOLUME 22, ISSUE 3, 2025, 12560 - 12572
DOI: https://doi.org/10.15282/ijame.22.3.2025.2.0959

RESEARCH ARTICLE

Optimization of Turning Parameters for Zirconia-Toughened Alumina-Based Self-Lubricating Composite Cutting Tool Materials Using Grey Relational Approach

Pujari Srinivasa Rao[1], Bagadi Pradeep Kumar[1,2]*, Dora Siva Prasad[1], Mathala Prithvi Raj[2], M. S. S. Srinivas Rao[2]

[1]GITAM (Deemed to be University), Gandhi Nagar, Rushikonda, Visakhapatnam, 530045, Andhra Pradesh, India
[2]Anil Neerukonda Institute of Technology & Sciences, Sangivalasa, Bheemunipatnam (Mandal), Visakhapatnam, 531162, Andhra Pradesh, India

ABSTRACT – Dry machining processes frequently encounter challenges, including increased cutting forces, high friction, and poor surface finishes, primarily due to the absence of lubrication. To address these issues, this study introduces the development of solid-lubricating cutting tools (SLTs) by incorporating elements such as Nichrome, silver, molybdenum, strontium sulfate, and calcium fluoride into a Zirconia Toughened Alumina matrix. The objective was to enhance the tribological performance of cutting tools for turning AISI 4340 steel under dry conditions. An experimental design based on the L8 mixed orthogonal array was employed, and the Grey-Taguchi analysis method was used to optimize multiple performance measures, including cutting forces, coefficient of friction, and surface roughness. Among the fabricated tools, SLT 4 exhibited superior performance. The results demonstrated a 73% reduction in cutting forces, a 45% decrease in the coefficient of friction, and a 66% improvement in surface finish compared to the unmodified base tool. These enhancements were attributed to the formation of a stable self-lubricating layer on the tool surface during machining. A confirmation experiment validated the optimization outcomes, confirming the effectiveness of the proposed tool composition.

ARTICLE HISTORY
Received : 31st Jan. 2025
Revised : 15th May 2025
Accepted : 30th May 2025
Published : 01st Sept. 2025

KEYWORDS
ZTA cutting tool
Coefficient of friction
Surface roughness
Grey relation analysis
Taguchi analysis

1. INTRODUCTION

Today, most of the research is motivated by enhancing the sustainability performance of cutting processes. In the machining industry, there is a growing need to meet elevated standards regarding the machined surface quality while minimizing environmental effects. Conventional machining practices, particularly those reliant on cutting fluids, have come under scrutiny due to their environmental hazards and health implications. Disposing of waste oils is a significant environmental risk in the manufacturing sector [1-6]. Moreover, the biological instability of cutting fluids fosters microbial growth, necessitating continuous monitoring to prevent health hazards. Under high-pressure and elevated temperature machining conditions, the cutting fluid may atomize and evaporate, leading to the formation of mist, which is an occupational hazard linked to respiratory ailments ranging from irritation to chronic illnesses such as asthma and even cancer. These concerns have catalysed a broader re-evaluation of machining practices. In this context, the adoption of Environmentally Sound Technologies (ESTs) has become central to industrial strategies aiming for operational sustainability [7]. Among emerging approaches, surface engineering techniques such as tool coating, surface texturing, and the development of self-lubricating tools have gained prominence for enabling dry or wet machining. Of these, self-lubricating cutting tools represent a particularly promising advancement. By embedding solid lubricants within tool materials or coatings, these tools eliminate the need for external cutting fluids, thereby mitigating the environmental and health risks associated with fluid use. This method not only aligns with sustainability goals but also enhances tool life and machining efficiency under dry conditions. Therefore, the current study situates itself within this evolving research landscape by critically examining the potential of self-lubricating cutting tools as a viable and scalable solution for achieving sustainable machining operations. In doing so, it contributes to the broader discourse on integrating green technologies into conventional manufacturing systems [8-11].

Dry cutting tools necessitate specific mechanical characteristics of hardness, composition, and temperature stability. These attributes cannot be attained with the commonly used cutting tools. Subsequently, ceramic tools produced via the powder metallurgy method were employed due to their customized properties. Comparatively normal, alumina (Al_2O_3) tools have the best mechanical properties and melting point temperature. Nonetheless, pure alumina cutting tools lack certain properties necessary for various speeds. Zirconia Toughened Alumina (ZTA) cutting tools have been widely adopted for machining. However, ZTA tools exhibit diminished tool life when utilized in dry conditions. Enhancing tool life can be achieved by incorporating elements that impart self-lubricating properties in dry environments. Researchers have identified calcium fluoride (CaF_2), molybdenum disulfide (MoS_2), strontium sulfate ($SrSO_4$), and tungsten disulfide (WS_2) as promising solid lubricants for this purpose [12-13]. Acchar et al. [14] fabricated a composite of Al_2O_3 with niobium carbide (NbC) 30 Wt.%, employing hot-pressing at 1700°C. Their investigation revealed a K_{1C} of 4.4 MPa·$m^{1/2}$

*CORRESPONDING AUTHOR | Bagadi Pradeep kumar | ✉ pradeep.me@anits.edu.in
© 2025 The Author(s). Published by Universiti Malaysia Pahang Al-Sultan Abdullah Publishing. This is an open access article under the CC BY-NC 4.0 International license

and a hardness of 20 GPa. The results revealed reduced tribological properties and increased mechanical properties compared to dry cutting with Al_2O_3/TiB_2 ceramic tools.

The following literature provides significant evidence of self-lubricating cutting tools machined with different workpieces, with their advantages. Deng Jianxin et al. [15] investigated the effects of incorporating CaF_2 solid lubricants into Al_2O_3/TiC ceramic cutting tools through hot pressing. Their analysis revealed a steady decrease in Alumina-based ceramic composites' Coefficient of Friction (COF) and wear resistance. Muthuraja et al. [16] evaluated the WC cutting tool. Among the tested materials, WC–Co–5 wt%. The percent CaF_2 demonstrated increased wear resistance and a low COF (0.25–0.28). Sharma et al. [17] employed a 4340 steel workpiece to turn textured SLTs. A lubricating layer on the rake face is beneficial in reducing COF and wear. The hybrid textured pattern filled with CaF_2 as a solid lubricant outperformed conventional plane tools across various cutting speeds.

Maintaining the cutting tools' hardness, toughness, and COF across different speeds, at low, medium, and high speeds, poses a challenge. At lower speeds, the generated heat was low, impeding the immediate propagation of heat into the zone where chips are formed. Hence, this heat generation is insufficient in the shear zone, leading to increased forces in different directions and changes in the tool geometry. In medium-range speeds, the lubricating layer on the rake surface is insufficient to achieve the desired wear resistance. However, when the temperature rises further, the tool properties further degrade [18-19]. Thus, there is a need to create cutting tools capable of operating effectively across a broad temperature span, ranging from room temperature (around 20 degrees Celsius) to temperatures exceeding 1000 degrees Celsius. This necessitates the integration of both tribological and mechanical properties. Optimization methods are crucial in enhancing performance assessments by identifying the significant cutting parameters.

Existing research on selecting optimal machining parameters seeks to enhance various performance metrics, primarily by extending tool life and reducing manufacturing duration. Bipin Kumar Singh et al. [20] investigated CuO modified ZTA ceramic inserts in dry turning operations. The incorporation of CuO led to better tribological properties. Several authors conducted a study on predicting surface roughness using ZTA cutting inserts through regression analysis. ANOVA results revealed that cutting speed has a significant effect on roughness. The findings indicated that cutting forces were affected by cutting velocity and feed. Grey relation analysis (GRA) optimizes machining parameters to enhance the machined components' productivity and surface quality [21-24].

Even though there is considerable advancement in the machining process, available literature falls short in addressing the development and performance evaluation of a single cutting tool capable of operating effectively across a range of cutting speeds. Furthermore, there is a notable lack of comprehensive experimental data on key performance indicators such as the COF, CF, and SR in the context of self-lubricating cutting tools. To address this gap, the present study focuses on the fabrication and performance evaluation of a modified Zirconia Toughened Alumina (ZTA) composite. The ZTA composite is reinforced with CaF_2, $SrSO_4$, Mo, Ag, and NiCr to enhance both its tribological and mechanical properties. These additives form a self-lubricating layer on the rake surface during machining, which reduces interfacial shear strength. The experimental investigation involves machining operations performed on an AISI4340 hardened steel to systematically measure COF, CF, and SR and identify the most influential variables in machining operations for a self-lubricating composite tool. Design of experiments employs an L8 mixed orthogonal array, while optimization of machining conditions uses Grey-Taguchi analysis.

2. MATERIALS AND METHODS

2.1 Materials Selection and Fabrication of Tools

The composite Al_2O_3-ZrO_2 (Y_2O_3) contains fixed amounts of NiCr and Ag, both set at 5% by weight, while CaF_2, Mo, and $SrSO_4$ vary between 5% and 10% by weight. 4 self-lubricating composite cutting tools were fabricated and compared to the Al_2O_3-ZrO_2 (Y_2O_3) tool, the elemental composition is selected based on the available literature [10, 11, 25-26]. These five sets of tools were fabricated using the powder metallurgy method. Table 1 shows the Tool grade of cutting tools and their compositions. Commercially available powders, including Al_2O_3 (60 microns), Ag (37 microns), CaF_2 (15 microns), Mo (44 microns), Ni (60 micron), Cr (46 microns), YSZ (5 mol%Y_2O_3) (30 microns), and $SrSO_4$ (31 microns), were selected to fabricate the tools. The raw materials were carefully selected based on the desired properties of the cutting tool. Once all the powders were prepared, they were thoroughly blended using a high-energy planetary ball milling machine (Capacity: 50–1600 rpm; Make: VB Ceramic Consultants, Chennai, Tamil Nadu). This mixing process ensured a homogeneous composition and consistent characteristics throughout the material. The blended powder was then loaded into a die and compacted under high pressure of 300 MPa using a compaction machine (Capacity: 60 Ton; Make: Thane, Maharashtra). A hardened steel die was employed to define the shape and dimensions of the cutting tool, as it can withstand the intense pressures involved. The compaction process was performed in multiple stages, with progressively increasing pressure to achieve optimal density and minimize internal voids. Following compaction, the tools were sintered in an OKAY electric furnace in an argon atmosphere at 1600°C (Maximum temperature: 1800 °C; Make: Bysakh Co., Calcutta). Sintering involves heating the compacted tools to a temperature just below the material's melting point, allowing the powder particles to fuse together and significantly reduce porosity, thereby enhancing the strength and density of the final product. After sintering, the tools were finished to the required shape and specifications using a tool and cutter grinder.

Table 1. Tool grade of cutting tools and their compositions (Al_2O_3-ZrO_2 (Y_2O_3) based composites)

Tool grade	Composition
SLT 1	Al_2O_3 -ZrO_2 (Y_2O_3)- NiCr-Ag-5$SrSO_4$-5Mo-5CaF_2
SLT 2	Al_2O_3 -ZrO_2 (Y_2O_3)- NiCr-Ag-5 $SrSO_4$-10Mo-10CaF_2
SLT 3	Al_2O_3 -ZrO_2 (Y_2O_3)- NiCr-Ag-10 $SrSO_4$-5Mo-10CaF_2
SLT 4	Al_2O_3-ZrO_2 (Y_2O_3)- NiCr-Ag-10 $SrSO_4$-10Mo-5CaF_2
Base tool (T_5)	Al_2O_3-ZrO_2 (Y_2O_3)

2.2 Experimental Conditions

The samples underwent machining using a CNC lathe. Cutting forces were recorded using a dynamometer. Machining trials were conducted for 20 minutes. The fabricated Self-lubricating ceramic cutting tools were tested at speeds of 50-275m/min with a speed gap of 75m/min. The feed was kept at 0.1 and 0.2 mm/rev, while the depth of cut was set to 0.1 and 0.2 mm.

2.3 Design of Experiments (DOE)

Design of Experiments (DOE) was employed to adjust input conditions to minimize the number of experiments needed to achieve desirable outcomes. Four ranges of speeds, two ranges of feed, and depth of cuts were included in the study. In this investigation, a mixed-level experimentation approach was adopted (4^1x2^2). The Taguchi L8 mixed orthogonal array was selected for its ability to provide sufficient results with a minimal number of experiments. The experiment was repeated thrice for each machining parameter set to obtain uniform values. The cutting forces were measured for uniformity from the experiments. The COF is calculated from the averaged cutting forces. A similar procedure was adopted in the measurement of surface roughness.

3. RESULTS AND DISCUSSION

3.1 Grey Relational Analysis (GRA)

The influence of machined parameters in the CNC turning of an AISI 4340 steel workpiece was analysed. Table 2 displays the measured and calculated COF, SR, and CF values for SLT 1 to SLT 4 and BT. Tables 3, 4, and 5 represent the calculated normalization data values, grey relational coefficients (GRC) values, and grey relational grade (GRG) values. In GRA, the optimization process is carried out in Figure 1 below.

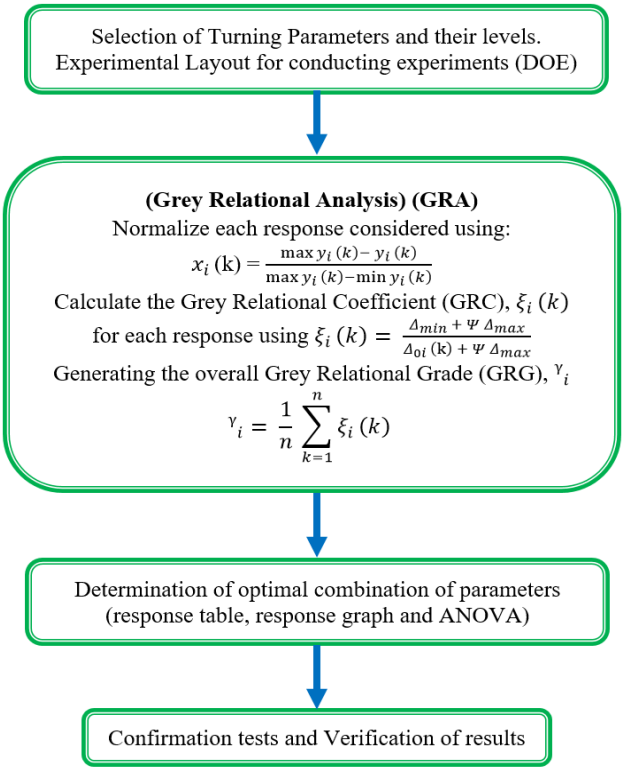

Figure 1. Flow chart for GRA experimental procedure

Table 2. Experimental values of SLTs and BT

V (m/min)	f (mm/ rev)	d (mm)	SLT 1					SLT 2					SLT 3					SLT 4					BT				
			COF	SR (µm)	ATF (N)	RTF (N)	MCF (N)	COF	SR (µm)	ATF (N)	RTF (N)	MCF (N)	COF	SR (µm)	ATF (N)	RTF (N)	MCF (N)	COF	SR (µm)	ATF (N)	RTF (N)	MCF (N)	COF	SR (µm)	ATF (N)	RTF (N)	MCF (N)
50	0.1	0.1	0.50	1.94	66	123	179	0.49	1.79	56	111	163	0.47	1.64	41	97	148	0.46	1.49	34	85	133	0.60	2.54	105	171	212
50	0.2	0.2	0.48	1.93	67	119	178	0.47	1.78	58	105	162	0.46	1.63	43	95	147	0.44	1.48	36	81	132	0.61	2.55	104	177	216
125	0.1	0.1	0.44	1.74	52	97	156	0.44	1.53	39	93	149	0.42	1.31	33	76	127	0.43	1.23	24	72	118	0.59	2.50	101	164	206
125	0.2	0.2	0.43	1.72	50	94	154	0.42	1.51	38	89	148	0.4	1.29	32	72	126	0.41	1.22	23	69	117	0.60	2.52	103	169	209
200	0.1	0.2	0.4	1.67	44	78	137	0.39	1.32	36	69	122	0.37	1.15	29	59	110	0.35	0.9	21	52	100	0.57	2.39	93	155	202
200	0.2	0.1	0.38	1.59	42	75	135	0.34	1.28	34	59	117	0.36	1.12	27	57	108	0.34	0.85	19	48	95	0.56	2.36	92	154	201
275	0.1	0.2	0.39	1.23	39	65	115	0.38	0.96	33	52	95	0.35	0.84	26	45	87	0.33	0.7	17	37	75	0.54	2.10	87	145	198
275	0.2	0.1	0.37	1.15	37	53	99	0.35	0.93	29	43	84	0.34	0.82	22	42	83	0.29	0.68	16	32	72	0.53	2.00	86	143	197

Table 3. Normalized data of SLTs and BT

V (m/min)	f (mm/ rev)	d (mm)	SLT 1					SLT 2					SLT 3					SLT 4					BT				
			COF	SR (µm)	ATF (N)	RTF (N)	MCF (N)	COF	SR (µm)	ATF (N)	RTF (N)	MCF (N)	COF	SR (µm)	ATF (N)	RTF (N)	MCF (N)	COF	SR (µm)	ATF (N)	RTF (N)	MCF (N)	COF	SR (µm)	ATF (N)	RTF (N)	MCF (N)
50	0.1	0.1	0.00	0.00	0.03	0.00	0.00	0.00	0.00	0.06	0.00	0.00	0.00	0.00	0.09	0.00	0.00	0.00	0.00	0.10	0.00	0.00	0.12	0.01	0.00	0.17	0.21
50	0.2	0.2	0.15	0.01	0.00	0.05	0.01	0.13	0.01	0.00	0.08	0.01	0.07	0.01	0.00	0.03	0.01	0.11	0.01	0.00	0.07	0.01	0.00	0.00	0.05	0.00	0.00
125	0.1	0.1	0.46	0.25	0.50	0.37	0.28	0.33	0.30	0.65	0.26	0.17	0.38	0.40	0.47	0.38	0.32	0.17	0.32	0.60	0.24	0.24	0.25	0.09	0.21	0.38	0.52
125	0.2	0.2	0.53	0.27	0.56	0.41	0.31	0.46	0.32	0.69	0.32	0.19	0.53	0.42	0.52	0.45	0.33	0.29	0.33	0.65	0.30	0.26	0.12	0.05	0.10	0.23	0.36
200	0.1	0.2	0.76	0.34	0.76	0.64	0.52	0.66	0.54	0.75	0.61	0.51	0.76	0.59	0.66	0.69	0.58	0.64	0.72	0.75	0.62	0.54	0.50	0.29	0.63	0.64	0.73
200	0.2	0.1	0.92	0.44	0.83	0.68	0.55	1.00	0.59	0.82	0.76	0.58	0.84	0.63	0.76	0.72	0.61	0.70	0.79	0.85	0.69	0.62	0.62	0.34	0.68	0.67	0.78
275	0.1	0.2	0.84	0.89	0.93	0.82	0.80	0.73	0.96	0.86	0.86	0.86	0.92	0.97	0.81	0.94	0.93	0.76	0.97	0.95	0.90	0.95	0.87	0.81	0.94	0.94	0.94
275	0.2	0.1	1.00	1.00	1.00	1.00	1.00	0.93	1.00	1.00	1.00	1.00	1.00	1.00	1.00	1.00	1.00	1.00	1.00	1.00	1.00	1.00	1.00	1.00	1.00	1.00	1.00

Table 4. Grey relational coefficient values of SLTs and BT

V (m/min)	f (mm/rev)	d (mm)	SLT 1					SLT 2					SLT 3					SLT 4					BT				
			COF	SR (μm)	ATF (N)	RTF (N)	MCF (N)	COF	SR (μm)	ATF (N)	RTF (N)	MCF (N)	COF	SR (μm)	ATF (N)	RTF (N)	MCF (N)	COF	SR (μm)	ATF (N)	RTF (N)	MCF (N)	COF	SR (μm)	ATF (N)	RTF (N)	MCF (N)
50	0.1	0.1	0.33	0.33	0.34	0.33	0.33	0.33	0.33	0.34	0.33	0.33	0.33	0.33	0.35	0.33	0.33	0.33	0.33	0.35	0.33	0.33	0.36	0.33	0.33	0.37	0.38
50	0.2	0.2	0.37	0.33	0.33	0.34	0.33	0.36	0.33	0.33	0.35	0.33	0.35	0.33	0.33	0.34	0.33	0.36	0.33	0.33	0.35	0.33	0.33	0.33	0.34	0.33	0.33
125	0.1	0.1	0.48	0.40	0.50	0.44	0.41	0.42	0.41	0.59	0.40	0.37	0.44	0.45	0.48	0.44	0.42	0.37	0.42	0.55	0.39	0.39	0.4	0.35	0.38	0.44	0.51
125	0.2	0.2	0.52	0.40	0.53	0.46	0.42	0.48	0.42	0.61	0.42	0.38	0.52	0.46	0.51	0.47	0.43	0.41	0.42	0.58	0.41	0.40	0.36	0.34	0.35	0.39	0.44
200	0.1	0.2	0.68	0.43	0.68	0.58	0.51	0.60	0.52	0.67	0.56	0.51	0.68	0.55	0.60	0.61	0.54	0.58	0.64	0.66	0.57	0.52	0.5	0.41	0.57	0.58	0.65
200	0.2	0.1	0.86	0.47	0.75	0.61	0.52	1.00	0.55	0.74	0.68	0.54	0.76	0.57	0.67	0.64	0.56	0.63	0.70	0.76	0.62	0.57	0.57	0.43	0.61	0.60	0.70
275	0.1	0.2	0.76	0.83	0.88	0.74	0.71	0.65	0.93	0.78	0.79	0.78	0.86	0.95	0.72	0.90	0.89	0.68	0.95	0.90	0.84	0.91	0.80	0.7	0.90	0.89	0.90
275	0.2	0.1	1.00	1.00	1.00	1.00	1.00	0.88	1.00	1.00	1.00	1.00	1.00	1.00	1.00	1.00	1.00	1.00	1.00	1.00	1.00	1.00	1.00	1.00	1.00	1.00	1.00

Table 5. GRG values of SLTs and BT

V (m/min)	f (mm/rev)	d (mm)	SLT 1		SLT 2		SLT 3		SLT 4		BT	
			GRG	Rank	GRG	Rank	GRG	Rank	GRG	Rank	GRG	Rank
50	0.1	0.1	0.335	8	0.337	8	0.339	7	0.339	8	0.359	7
50	0.2	0.2	0.338	7	0.340	7	0.337	8	0.3391	7	0.336	8
125	0.1	0.1	0.439	6	0.448	6	0.454	6	0.444	6	0.426	5
125	0.2	0.2	0.457	5	0.462	5	0.472	5	0.460	5	0.385	6
200	0.1	0.2	0.552	4	0.569	4	0.580	4	0.601	4	0.558	4
200	0.2	0.1	0.591	3	0.630	3	0.617	3	0.667	3	0.589	3
275	0.1	0.2	0.793	2	0.823	2	0.867	2	0.903	2	0.859	2
275	0.2	0.1	1.000	1	1.000	1	1.000	1	1.000	1	1.000	1

3.2 Cutting Forces

Cutting forces are beneficial in assessing the effect of SLTs in dry cutting. In SLTs, adding the lubricating elements improves mechanical and tribological properties. In the present investigation, cutting force values were higher in the base tool than in the self-lubricating cutting tools. The chips, which are identified in Figure 2, are base cutting tool discontinuous chips. In contrast, SLTs form continuous chips with less helical shapes, which is one of the reasons for reducing heat generation in SLTs. Figures 3, 4, and 5 show the various cutting tools' hardness, density, and porosity values. The SLT 1 cutting tool, characterized by low weight percentages of Mo and $SrSO_4$, showed limited synergistic enhancement of mechanical properties. Its comparatively low hardness (1502 HV) likely contributed to increased tool wear, resulting in unstable and fluctuating cutting forces during operation. In the SLT 2tool, the Mo content was increased from 5% to 10%, which led to an improvement in hardness relative to SLT 1. However, its hardness remained lower than that of the SLT 3 and SLT 4 tools. Consequently, a slight reduction in cutting forces was observed with SLT 2, attributed to the increased Mo content. The SLT 3 tool, with a higher weight percentage of CaF_2, experienced a reduction in hardness compared to SLT 4, which may have adversely affected its performance.

Additionally, porosity was progressively reduced from SLT 1 to SLT 4. This decrease in porosity contributed to improved edge integrity by making the tool edges less susceptible to chipping and rounding, thereby reducing cutting forces. Lower porosity also enhanced heat dissipation within the tool, mitigating thermal softening and wear, further contributing to the observed reduction in cutting forces. The properties of all the cutting tools were better for SLT 4 and poorer for the base tool. This is also the reason for reducing the cutting forces in SLT 4. SEM images of the chip morphology of self-lubricating cutting tools are shown in Figures 6(a) to 6(d), and the base cutting tool is shown in Figure 6(e). SEM images of the chips after analysis of the base tool when exposed to higher working conditions, large serrations are present on the chip, leading to higher plastic deformation. In case of SLTs, lesser cutting force values were observed because of serrations and scratches on the chips, which were gradually reducing until SLT 4 (Figure 6(d)); hence, SLT 4 cutting force values were reduced because of less heat generation present on the chip, which indicates lesser plastic deformation moreover, as the effectiveness of the lubricating film improves from SLT 1 to SLT 4, the efficiency of cutting tools.

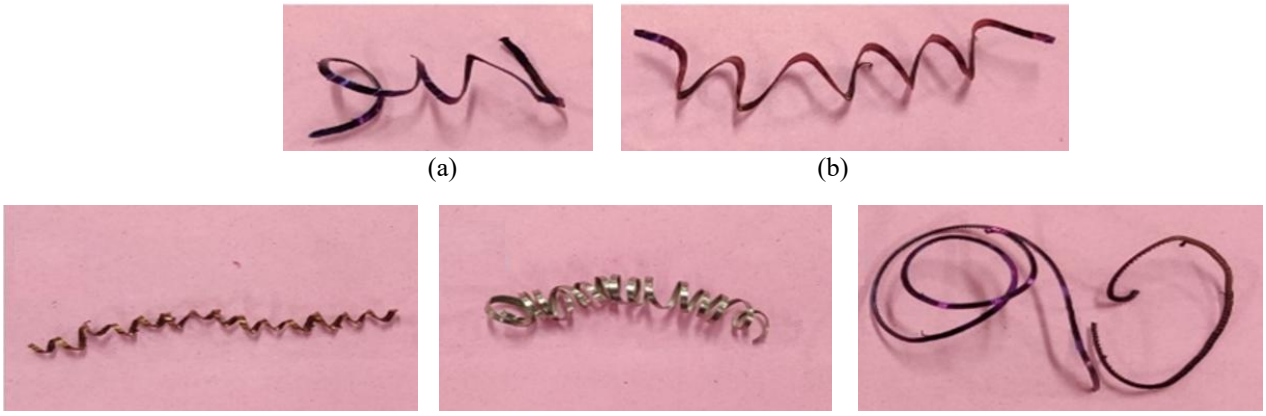

Figure 2. Machined chips of: (a) SLT 1, (b) SLT 2, (c) SLT 3, (d) SLT 4, and (e) BT

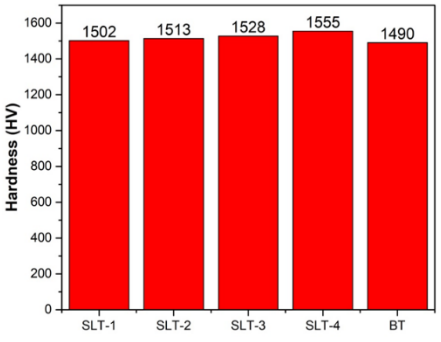

Figure 3. Hardness of various cutting tools

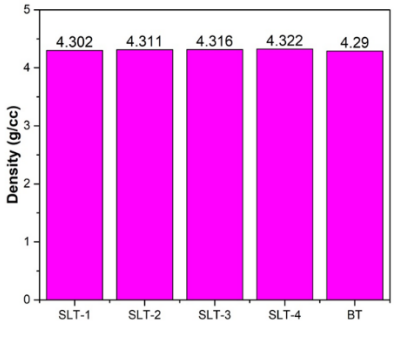

Figure 4. Density of various tools

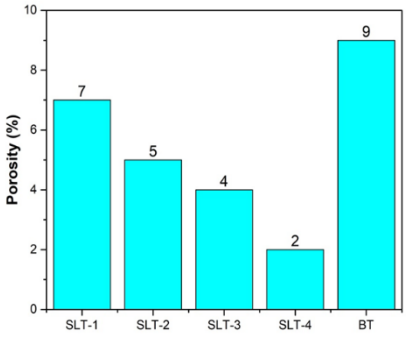

Figure 5. Porosity of various tools

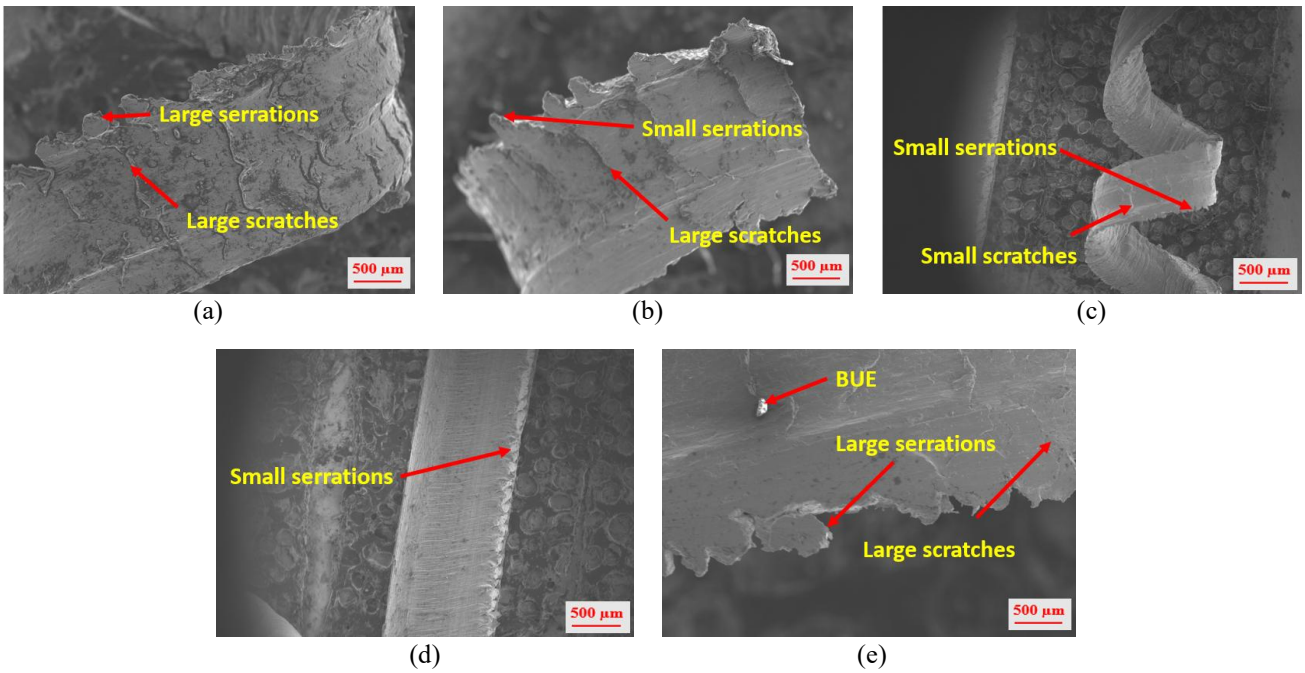

Figure 6: SEM of chips with cutting tools; (a) SLT 1, (b) SLT 2, (c) SLT 3, (d) SLT 4, and (e) BT

3.3 Coefficient of Friction

The coefficient of friction (COF) is calculated by using the equation (1)

$$\mu = \tan(\alpha + \arctan\left(\frac{F_y}{F_z}\right)) \quad (1)$$

where μ = COF, α= Rake angle, F_y = Radial Thrust Force (RTF) and F_z = Main Cutting Force (MCF). Table 2 displays the calculated values of COF across various speeds. These values exhibit SLT 4 as the better cutting tool due to its low COF, consistent with earlier explanations emphasizing its superior lubrication mechanism. High hardness and consistent edge geometry reduce tool-workpiece adhesion and minimize ploughing effects during cutting. Meanwhile, low porosity results in a smoother, more uniform tool surface, which lowers friction by limiting micro-asperities. The improved material integrity also inhibits the formation of built-up edge (BUE), a key factor that contributes to increased friction in tools with inferior mechanical properties. In hard machining, the hardness of the workpiece leads to significant cutting forces, resulting in substantial tool wear. The lubrication effect is crucial in the effect produced at the heat generation zone.

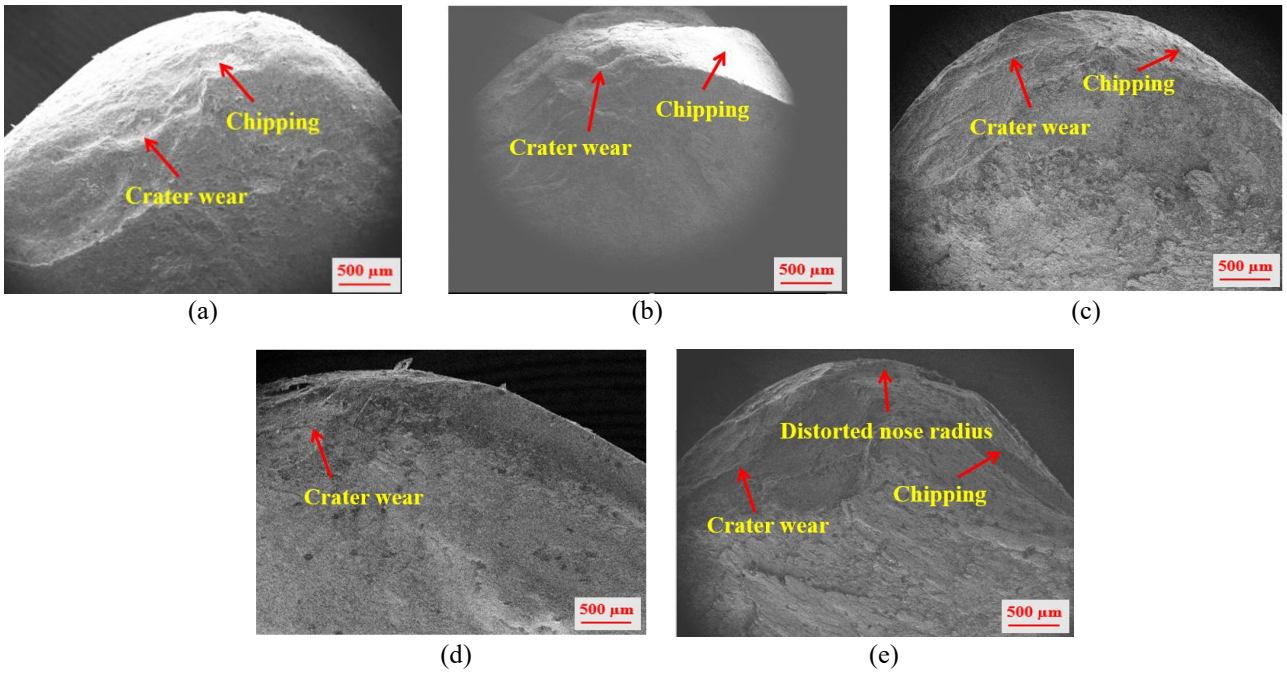

Figure 7. SEM images for the crater face of (a) SLT 1, (b) SLT 2, (c) SLT 3, (d) SLT 4, and (e) BT

Figure 7 presents the SEM of the crater wear face for both SLTs and base tools. The SEM images of the crater face for SLTs reveal the extent of chipping and wear during machining. These findings indicate a gradual reduction in edge chipping from SLT 1 to SLT 3, with no occurrence in SLT 4 (Figures 7(a) to 7(d)). SLTs are typically employed at a high range of machining speeds due to elevated temperatures, which soften the material and prompt the formation of a lubricating film. This film mitigates tool wear. Machining with SLT 1 resulted in more pronounced chipping and crater wear, suggesting a less effective lubrication phenomenon (Figure 8(a)). Conversely, SLT 2 (Figure 7(b)) and SLT 3 (Figure 7(c)) exhibit reduced wear and chipping, indicating a relatively more effective lubricating film, as depicted in Figures 8(b) and 8(c). The efficacy of the lubricating film at the tool rake face of SLT 4 is better than that of other tools (Figure 8(d)). The base tool does not contain the lubricating elements; obviously, the heat generation was higher, which leads to flank wear and fracture surface occurring (Figure 8(e)), and is also exposed to elevated speeds, resulting in distorted nose radius forms, which indicates higher deformation, as displayed in Figure 7(e).

3.4 Surface Roughness

The surface roughness achieved during machining reflects the surface quality, which is crucial for the effectiveness of machined components to some degree. The machining parameters and characteristics of the cutting tool influence surface quality, particularly the lubrication effect at the tool-work junction. A sharp and stable cutting edge, maintained by the tool's high hardness and low porosity, helps prevent material tearing and minimizes vibration-induced surface marks. The combination of lower cutting forces and reduced coefficient of friction (COF) leads to decreased tool deflection, resulting in fewer surface irregularities. Additionally, minimal formation of built-up edge (BUE) ensures that the genuine cutting edge, rather than adhered material, engages the workpiece, producing a more precise and smoother machined surface. This study compares SLTs with BT regarding surface irregularities across different machining parameters. Figure 8 shows SEM micrographs of the tool flank face in the wear tracks.

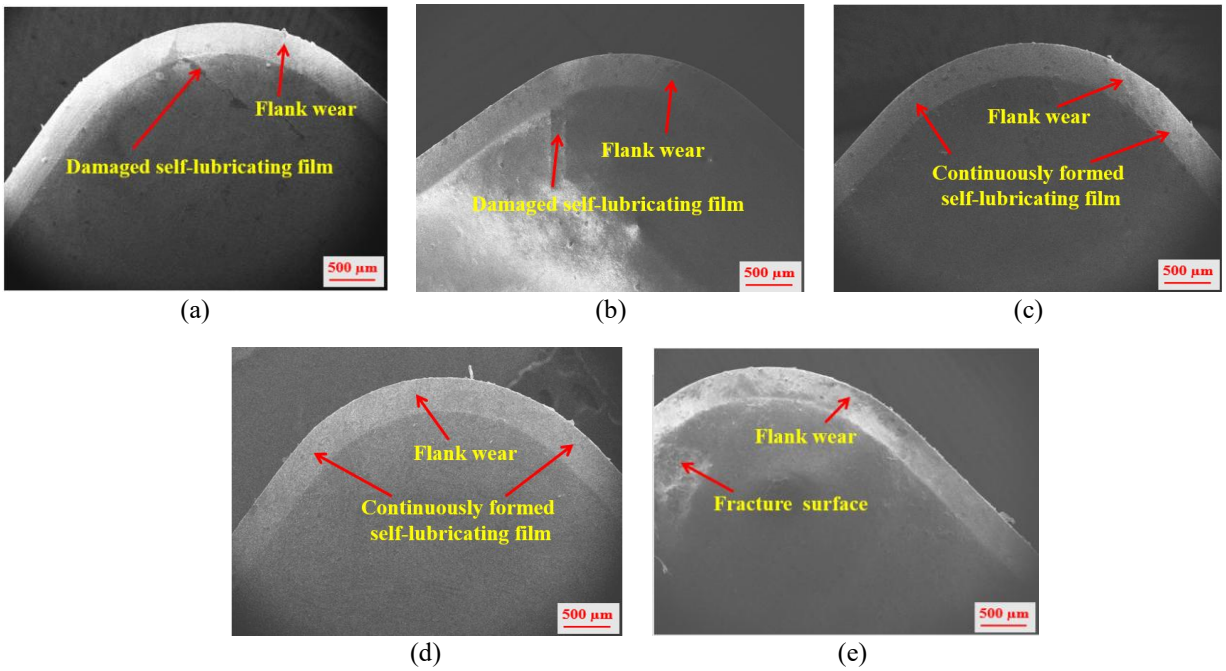

Figure 8. SEM micrographs in the tool flank face of (a) SLT 1, (b) SLT 2, (c) SLT 3, (d) SLT 4, and (e) BT

In Figure 8(a), we observe that the flank wear of SLT 1 is expected as the lubricating layer, which occurs during cutting, is compromised. It negatively affects the machined surface quality and wear resistance, leading to a decline in component surface finish. Similar characteristics are seen in SLT 2, SLT 3, and SLT 4 as depicted in Figures 8(b-d). Comparatively, the tool wear is significantly reduced in SLT 4, making it the most effective tool compared to SLTs. Figure 8(e) displays the BT, which lacks lubrication and has undergone more damage. COF and CF are at their maximum, resulting in higher flank wear and fracture surface levels than SLTs.

Figure 9(a-b) shows the machined surface produced using SLT 1, which displays plowing grooves, metal debris, smearing phenomenon, and surface tearing. This occurs as the cutting tool adheres to the cutting region under increased forces, resulting in elevated temperatures. Figure 9(c) depicts the microstructure of the machined surface obtained using SLT 2. Micro-particle deposits are Visible on the machined surface. As mentioned earlier. The accumulation of micro-particles was noted, particularly at high cutting speeds. Increased speeds lead to higher strain rates in the distortion zones, causing chips to fragment into small particles that deposit across the machining area. Additionally, these micro-particles cause increased tool wear and BUE. The machined surface produced by the SLT 3 composite cutting tool displays feed marks in Figure 9(d). Feed mark impressions typically arise during single-point turning in a machining area. Figure 9(e) presents the machined surface generated by SLT 4, where only feed marks are apparent, which is standard. On the contrary, the machined surface generated by the base tool exhibits scratch marks and burnishing layers, as shown in Figure

9(f). Scratch marks occur due to material softening caused by the extrusion effect. The extensive side-flow can be ascribed to higher temperatures. Additionally, the elevated temperatures lead to surface burning and the tool tip failure.

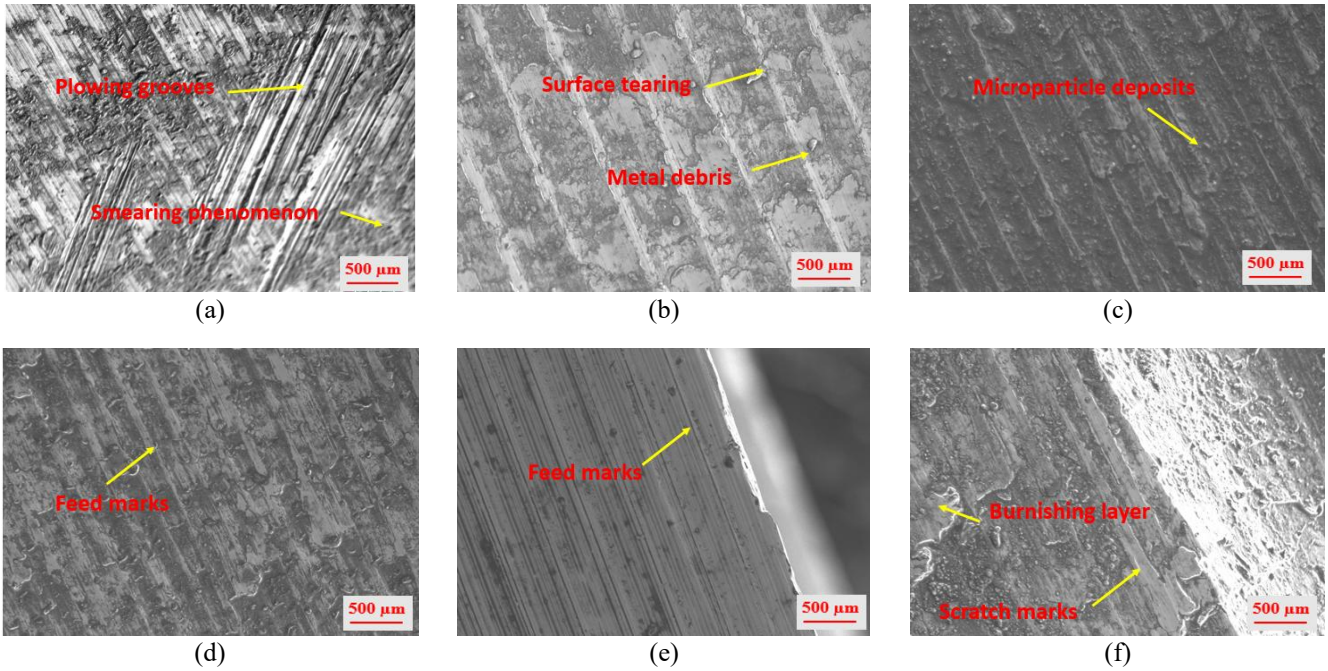

Figure 9: Scanning electron micrographs of machined surface defects of (a) & (b) SLT 1, (c) SLT 2, (d) SLT 3, (e) SLT 4, and (f) BT

3.5 Analysis of Variance

Previous studies on dry machining of various cutting tools have commonly utilized input conditions to understand the adverse effect on various output parameters. As shown in Table 6, it was observed that SLTs and BT achieve optimized values for GRG. SLT 4 stands out as the best performance measure under these conditions. Table 6 presents the Analysis of Variance (ANOVA) for CC_i of SLT 4. ANOVA was performed at a 95% confidence level. The F-value of 0.143091 for the cutting speed in the SLT 4 tool indicates a significant impact, with a P-value of 0.001. This provides strong statistical evidence that cutting speed significantly influences the process. The P and the F-value of 0.036 and 0.003928 for the feed rate indicate a significant effect. The F and p-values of 0.002682 and 0.05 suggest a considerably low impact on the depth of the cut.

The p-value from the F-Test (Table 7) is observed to be 0.00065, which is very low and less than the α-value (0.05), indicating that the process parameters have a statistically significant effect on responses. The strong collective influence of the process parameters is further confirmed by the high F-value.

Table 6. ANOVA for GRG of SLT 4

Source	DOF	SS	MS	F	P	% Contribution
V	3	0.429272	0.429272	0.143091	0.001	98.410
f	1	0.003928	0.003928	0.003928	0.036	0.900
d	1	0.002682	0.002682	0.002682	0.050	0.614
Residual Error	2	0.000302	0.000302	-	-	0.076
Total	7	0.436185	-	-	-	100.000

Table 7. F-Test

Source	SS	df	MS	F	p-value
Between Groups	200.13	3	66.71	9.73	0.00065
Within Groups	109.66	16	6.85		
Total	309.79	19			

Effect Size (η^2) is calculated using Equation (2), which is approximately 64.6%. The large effect size indicates that 65% of the total variance in the responses is explained by speed, feed and depth of cut, which is substantial.

$$\eta^2 = \frac{SS_{between}}{SS_{total}} \quad (2)$$

The within-group variability MSE is 6.85. The relatively low MSE compared to the MS between groups reinforces the strength of the treatment effect or group difference.

3.6 GRA Confirmation Experiment

The optimal cutting conditions of Grey relational grade value (GRG) were identified from the mean compelling plots, as depicted in Figure 10. Figures 10(a) to 10(e) indicate that V at level 4, f at level 2, and d at level 1 were the most effective parameters for SLT 1 to SLT 4 and the base tool, resulting in lower performance measures. The validation experiment presented in Table 8 serves as significant evidence. SLT 4 emerged as the top-performing cutting tool. The main effect plot analysis identified the optimal input parameter combination of V, f, and d levels (V4f2d1) for SLT 4. The projected and actual machining performance exhibited good agreement, with the CCi value increasing by 0.556 for SLT 4.

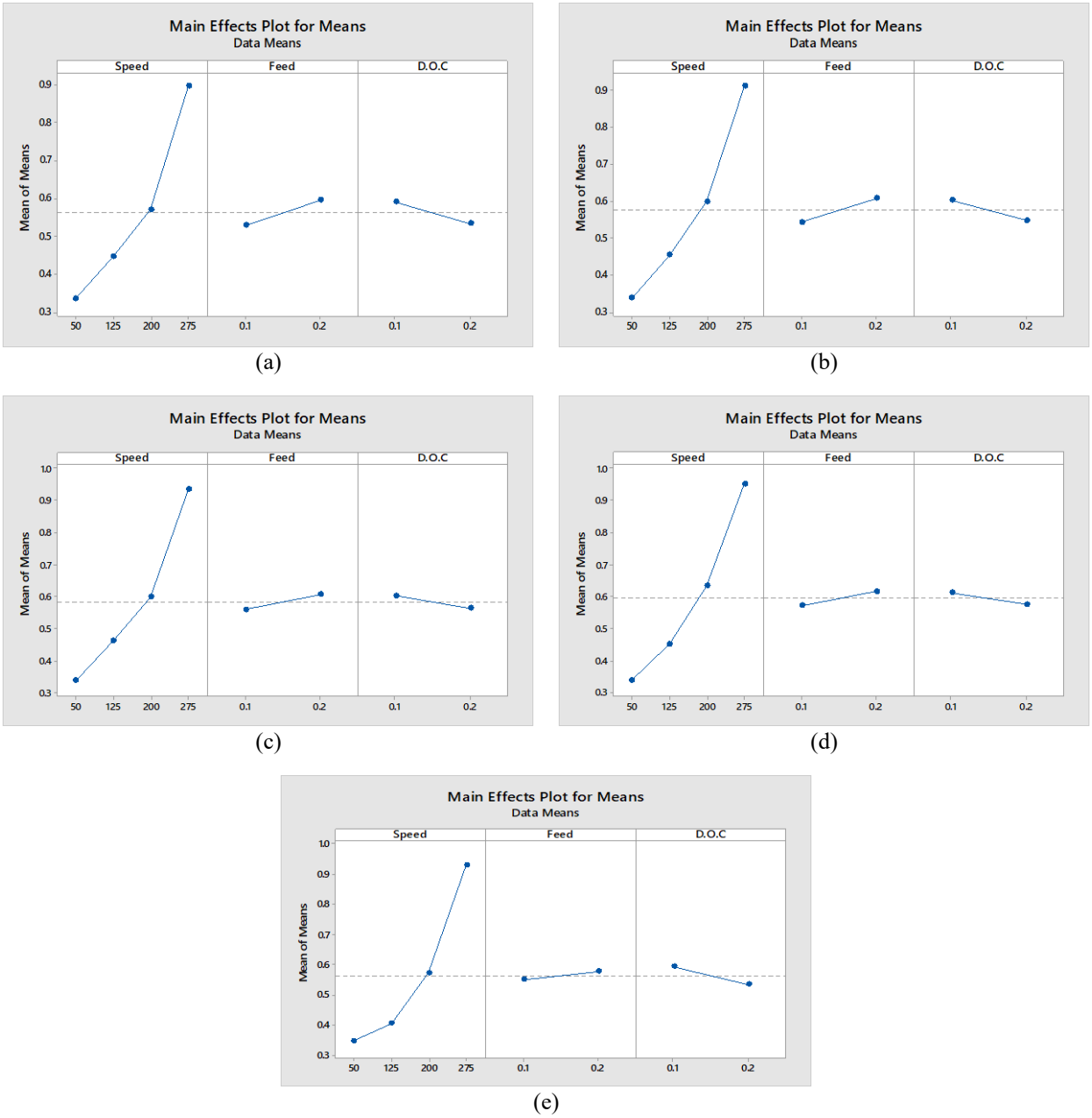

Figure 10. Main effects plot for Grey relational grade of (a) SLT 1, (b) SLT 2, (c) SLT 3, (d) SLT 4, and (e) BT

Table 8. Validation experiment of SLT 4

Output parameters	SLT 4cutting tool		
	Initial input conditions	Optimal cutting conditions	
		Prediction	Experiment
	$V_2f_1d_1$	$V_4f_2d_1$	$V_4f_2d_1$
COF	0.428	-	0.289
SR	1.29	-	0.68
ATF	23.9	-	15.9
RTF	71.8	-	31.9
MCF	117.9	-	71.7
GRG	0.444	0.992189	1
Improvement in GRG		0.556	

4. CONCLUSIONS AND FUTURE SCOPE

In this investigation, SLTs with different elements were fabricated and compared with BT. The following reasons can be made. The best permutation of ZTA based on adding solid-lubricating materials, viz., Ag, Mo, $SrSO_4$, NiCr, and CaF_2, i.e., SLT 4, is a unique cutting tool over a wide range of cutting speeds. The fabricated SLTs were identified to have reduced wear, chipping, and surface defects compared to BT. The optimum values for the SLT 4 are the performance measures like COF-0.289, SR-0.68µm, ATF-15.9N, RTF-31.9N, and main cutting force-71.7N. Further, SLT 4 showed significant improvement with an improvement of GRG value (0.556) through the GRA method and the order alternatives as E8>E7>E6>E5>E4>E3>E2>E1. The superior performance of the SLT 4tool can be primarily attributed to its higher content of Mo and $SrSO_4$, which enhanced the tool's hardness and reduced its porosity. Additionally, the formation of a uniform and continuous self-lubricating film on the tool surface further contributed to its improved functional properties. The present study effectively optimized turning parameters for ZTA-based self-lubricating composite cutting tools using Grey Relational Analysis (GRA) in conjunction with the Taguchi method. For future research, the integration of advanced optimization techniques such as Response Surface Methodology (RSM), Artificial Intelligence (AI) approaches including genetic algorithms, neural networks, and machine learning models, and multi-objective evolutionary algorithms (e.g., NSGA-II) can be explored to enable predictive modeling and adaptive learning, as well as to achieve Pareto-optimal solutions. Additionally, advanced tool characterization techniques, such as SEM-EDS mapping, nanoindentation, and thermal conductivity analysis, can provide deeper insight into the influence of tool composition and porosity on performance parameters like tool wear, built-up edge (BUE) formation, and heat dissipation. Furthermore, conducting long-term machining trials under varying cutting conditions (e.g., dry, minimum quantity lubrication [MQL], and cryogenic environments) would help in evaluating wear mechanisms and developing wear models specific to ZTA-based tools with different self-lubricating phases.

ACKNOWLEDGMENTS

We would like to thank the management of GITAM Deemed to be University, Visakhapatnam, for their invaluable support in providing the laboratory equipment to complete the experiments. We are also grateful to the team at TUV Labs, who provided us with the Field Emission Scanning Electron Microscopy (FESEM) facility available in AMTZ, Visakhapatnam, for getting quality images.

CONFLICT OF INTEREST

The article was sent for publication in the journal. The authors have no conflicts of interest. This is the original work of the authors and has not been previously published in other publications.

AUTHOR CONTRIBUTION:

P. Srinivasa Rao: Writing paper and experiments

B. Pradeep Kumar: Data analysis

D. Siva Prasad: Paper framework

M. Prithvi Raj: Result analysis

M.S.S. Srinivasa Rao: Experiments

REFERENCES

[1] J. X. Deng, X. Ai, and Y. H. Feng, "Wear lubrication and matching of cutting tools with the workpiece materials," *Chinese Journal of Mechanical Engineering*, vol. 38, no. 4, pp. 40–45, 2002.

[2] S. H. Musavi and B. Davoodi, "Risk assessment for hazardous lubricants in machining industry," *Environmental Science and Pollution Research*, vol. 28, no. 9, pp. 625–634, 2021.

[3] R. M. Park, "Risk assessment for metalworking fluids and cancer outcomes," *American Journal of Industrial Medicine*, vol. 61, no. 3, pp. 198–203, 2018.

[4] V. Kumar,and A.K. Choudhary, "A hybrid response surface methodology and multi-criteria decision making model to investigate the performance and emission characteristics of a diesel engine fueled with phenolic antioxidant additive and biodiesel blend's, *Journal of Energy Resources Technology*, vol. 145, no. 9, pp. 1-22, 2023.

[5] M. K. Sinha, A. Pal, K. Kishore, A. Singh, Archana, H. Sansanwal, et al., "Applications of sustainable techniques in machinability improvement of superalloys: a comprehensive review," *International Journal on Interactive Design and Manufacturing*, vol. 17, no. 1, pp. 473–498, 2023.

[6] S. H. Musavi and B. Davoodi, "Risk assessment for hazardous lubricants in machining industry," *Environmental Science and Pollution Research International*, vol. 28, no. 1, pp. 625-634, 2021.

[7] G. S. Kadam and R. S. Pawade," Cutting force assessment in HSM of Inconel 718 aided with water vapour as an eco-friendly cutting fluid," *Recent Advancements in Manufacturing Processes*, vol. 1, no. 1, pp. 243-251, 2022.

[8] X. Mu, Z. Chen, H. Chen, X. Meng, G. Xiao, M. Yi, et al., "Mechanism of improving the surface integrity of self-lubricating ceramic tool in cutting nickel-based alloy," *International Journal of Refractory Metals and Hard Materials*, vol. 1, no. 1, pp. 1072-1098, 2025.

[9] M. Yi, L. Zhao, Z. Zhang, Y. Yu, Y. Bao, J. Wang, et al., "Development of (W,Ti,Ta)C/CaF_2 nano-self-lubricating cermet tool and its dual lubrication cutting mechanism," *Applied Ceramic Technology*, vol. 22, no. 3, pp. 1-13, 2025.

[10] Z. Sheng, H. Zhu, Y. He, B. Shao, Z. Sheng, and S. Wang, "Tribological effects of surface biomimetic micro–nano textures on metal cutting tools: A review," *Biomimetics*, vol. 10, no. 5, pp. 1-11, 2025.

[11] B.K. Singh, S. Goswami, K. Ghosh, H. Roy, and N. Mandal, "Performance evaluation of self lubricating CuO added ZTA ceramic inserts in dry turning application," *International Journal of Refractory Metals and Hard Materials*, vol. 98, no. 4, pp. 1-13, 2021.

[12] W. Acchar and A. M. Segadães, "Properties of sintered alumina reinforced with niobium carbide," *International Journal of Refractory Metals and Hard Materials*, vol. 27, no. 2, pp. 427–430, 2009.

[13] D. M. Kim, I. Lee, S. K. Kim, B. H. Kim, and H. W. Park, "Influence of a micro patterned insert on characteristics of the tool-workpiece interface in a hard turning process," *Journal of Materials Processing Technology*, vol. 229, no. 3, pp. 160–171, 2016.

[14] M. Law, R. Karthik, S. Sharma, and J. Ramkumar, "Finish turning of hardened bearing steel using textured PcBN tools," *Journal of Manufacturing Processes*, vol. 60, no. 1, pp. 144–161, 2020.

[15] D. Jianxin, L. Lili, Y. Xuefeng, L. Jianhua, S. Junlong, and Z. Jinlong, "Self-lubrication of Al_2O_3/TiC/CaF_2 ceramic composites in sliding wear tests and in machining processes," *Materials and Design*, vol. 28, no. 3, pp. 757–764, 2007.

[16] A. Muthuraja and S. Senthilvelan, "Development of tungsten carbide based self-lubricant cutting tool material: Preliminary investigation," *International Journal of Refractory Metals and Hard Materials*, vol. 48, no. 1, pp. 89–96, 2015.

[17] V. Sharma and P. M. Pandey, "Comparative Study of turning of 4340 hardened steel with hybrid textured self-lubricating cutting inserts," *Materials and Manufacturing Process*, vol. 31, no. 14, pp. 1904–1916, 2016.

[18] G. S. Kadam and R. S. Pawade, "Water Vapour assisted machining of Inconel 718 incorporating through-tool cutting fluid delivery approach," *International Journal on Interactive Design and Manufacturing*, vol. 18, no. 10, pp. 7317-7331, 2023.

[19] G. S. Kadam and R. S. Pawade, "Water vapor cutting fluid assisted productive machining of Inconel 718," *Materials and Manufacturing Process*, vol. 39, no. 1, pp. 1-12, 2024.

[20] B. K. Singh, S. Goswami, K. Ghosh, H. Roy, and N. Mandal, "Performance evaluation of self-lubricating CuO added ZTA ceramic inserts in dry turning application," *International Journal of Refractory Metals and Hard Materials*, vol. 98, no. 1, pp. 1-8, 2021.

[21] P. Sharma, K. Kishore, V. Singh, and M. K. Sinha, "Optimization of process parameters for better surface morphology of electrical discharge machining-processed Inconel 825 using hybrid response surface methodology-desirability function and multi-objective genetic algorithm approaches," *Journal of Materials Engineering and Performance*, vol. 1, no. 1, pp. 1-18, 2023.

[22] N. J. Rathod, M. K. Chopra, S. N. Shelke, P. K. Chaurasiya, R. Kumar, K. K. Saxena, et al., "Investigations on hard turning using SS304 sheet metal component grey based Taguchi and regression methodology," *International Journal on Interactive Design and Manufacturing*, vol. 5, no. 1, pp. 2653-2664, 2023.

[23] B. Karnan, A. Kuppusamy, T. P. Latchoumi, A. Banerjee, A. Sinha, A. Biswas, et al., "Multi-response optimization of turning parameters for cryogenically treated and tempered WC–Co inserts," *Journal of the Institution of Engineers (India) Series D*, vol. 103, no. 4, pp. 1-12, 2024.

[24] M. P. Raj, A. K. Pramanick, and M. Kumar, "Parametric optimization in co-axial laser powder deposition of cobalt-base alloys on DIN 1.2714 die steel," *Proceedings of the Institution of Mechanical Engineering science Part C*, vol. 238, no. 1, pp. 543-556, 2024.

[25] L. Kong, Q. Bi, S. Zhu, J. Yang, and W. Liu, "Tribological properties of ZrO_2 -Y_2O_3 -Mo-BaF_2/CaF_2 composites at high temperatures," *Tribology International*, vol. 45, no. 1, pp. 43–49, 2012.

[26] F. Liu, Y. Zhou, X. Zhang, W. Cao, and J. Jia, "Tribological properties of NiCr–ZrO_2 (Y_2O_3)–$SrSO_4$ composites at elevated temperatures," *Ceramics International*, vol. 42, no. 11, pp. 12981–12987, 2016.